Egypt. J. Chem. **59**, No.4, pp.609 – 621 (2016)

Preparation and Characterization of Micro-Porous ZnO Nanoparticles

Asmaa S. Morshedy*[1], Ahmed M.A. El Nagger[1], Sahar M. Tawfik[1], Omar I. Sif El-Din[1], Sana I. Hassan[1] and Ahmed I. Hashem[2]

[1]Egyptian Petroleum Research Institute, Nasr City and [2]Chemistry Department, Faculty of Science, Ain Shams University, Cairo, Egypt.

ZnO nanoparticles (NPs) have been synthesized by precipitation method and auto-ignition method from zinc nitrate hexahydrate. The powder was characterized by thermal analysis (TGA-DTA), X-ray diffraction (XRD), scanning electron microscopy (SEM), transmission electron microscopy (TEM), Ultra violet- Visible optical absorption (Uv-Vis), and photoluminescence spectroscopy analyses (PL). XRD patterns for both catalysts showed that ZnO nanoparticles have hexagonal unit cell structure. SEM and TEM pictures detect the morphology and particle size of the as-prepared ZnO NPs. The UV-Vis absorption spectrum shows ZnO nanoparticles prepared by precipitation method has an absorption band at 385 nm while by auto-ignition method has an absorption band at 355nm. PL spectra proved that ZnO prepared by auto-ignition method was the most active one. This indicated a minimum recombination rate. These ZnO nanoparticles can be used in different applications due to their great optical properties.

Keywords: ZnO nanoparticles (NPs), Uv-Vis absorption and Photolumin-ancesence (PL).

Today, there has been an increasing demand for the development of nanosized semiconductors due to their considerable electrical and optical properties which are highly useful in fabricating nanoscaled optoelectronic and electronic devices with multifunctionality[1-3]. Among various semiconducting materials, zinc oxide (ZnO) is a distinctive electronic and photonic wurtzite n-type semiconductor with a large direct band gap of 3.37 eV and a prominent exciton binding energy (60 meV) at room temperature[4.5]. ZnO nanoparticles are promising candidates for various applications, such as solar cells[6] , nanogenerators[7], bio-sensors[8], varistors[9], gas sensors[10], photo-detectors[11], and photo-catalysts[12]. From the literature survey, it was found that various approaches for the synthesies of ZnO NPs have been developed, namely, sol-gel[13] , thermal decomposition of organic precursor[14], microemulsion[15], spray pyrolysis[16], electrodeposition[17], microwave- assisted techniques[18] , ultrasonic[19], chemical vapor deposition[20] , hydrothermal[21] and precipitation methods[22-23]. Most of these techniques were

*Corresponding author: Email address: asma_2000asma@yahoo.com (asmaa said morshedy) Tel.: 00201095036044

not extensively used on a huge scale, but chemical synthesis has been widely used due to its simplicity and lower cost. In the present study, we report the preparation of ZnO nanoparticles using chemical precipitation[24] and auto-ignition [25] methods. The characterization of ZnO nanoparticles using different analytical tools is discussed.

Experimental

Instruments

The as-prepared ZnO nanoparticles from the two methods were characterized for their optical, morphological and nano-structural properties through various analysis tools. Differential thermal analysis was carried out by Q600 DST simultaneous DSC/TGA apparatus. All runs were carried out at a heating rate of 10ºC/min in the temperature range from room temperature to 1000ºC under air flow to follow the structural changes accompanying the thermal treatment. The X-ray diffraction patterns of both oxides were recorded by Brucker AXS-D8 Advance XRD instrument (Germany) with nickel-filtered copper radiation (λ =1.5405Å) at scanning speed of 0.4 degrees/ min. The N_2 adsorption-desorption isotherms were performed with Quantachrome Nova 3200 instrument (USA). The surface area and total pore volume were calculated throughout the BET plot and BJH equation, respectively. The surface, as well as the inner morphology of the prepared oxides, was obtained by scanning electron microscope (SEM) model JEOL 5300 (Japan) and Transmission electron microscope (TEM), model JEOL 1230, Japan. The UV- reflectance analysis of the prepared photocatalysts was acquired via UV-spectrophotometer model V-570 manufactured by JASCO (Japan). Photo-luminance (PL) analysis (as one of the essential characteristics for photocatalysts) was measured at room temperature using Spectrofluorometer, model JASCO FP-6500-Japan.

The zinc Oxide (ZnO) nanoparticles were prepared by two methods namely;
(a) The chemical precipitation and (b) The auto-ignition methods.

(a) In the chemical precipitation, 0.1N solution of Zn $(NO_3)_2$.6 H_2O was prepared using de-ionized water. The solution was then heated up to 60 ^oC to enhance the dissolution of the zinc salt. An aqueous solution of NaOH (0.5N) was afterward added drop-wise to the zinc solution under vigorous stirring until the reaction had completed. During the addition of NaOH, a cloud of suspended molecules was initially observed. The solution was then turned to bright white due to the formation of the Zn-hydroxide particles. The stirring was afterward stopped, and the hydroxide particles were allowed to precipitate at the bottom of the preparation vessel. The precipitate was then filtered on a Buchner funnel and repeatedly washed with de-ionized water. The obtained zinc hydroxide was dried in an oven for overnight at 120 ^oC. Finally, the hydroxide particles were converted to Zn-oxide (catalyst A) via a calcination step for 4 hr at 500 ^oC.

(b) In auto-ignition, zinc nitrate [Zn $(NO_3)_3.6H_2O$] and citric acid ($C_6H_8O_7.H_2O$) were first dissolved in a minimum volume of de-ionized water on a different basis. Both solutions were then mixed with certain molar ratios (according to equation 1). The mixing was executed at 80^o C under energetic stirring 600 rpm.

$$9\ Zn(NO_3)_2.4H_2O_{(c)} + 5\ C_6H_8O_{7\,(c)} \longrightarrow 9\ ZnO_{(C)} + 9\ N_{2\,(g)} + 30\ CO_{2\,(g)} + 24\ H_2O_{(g)}$$ eq. (1)

At the first place, a transparent solution was detected while a highly viscous snow-white liquid was then obtained after a short time (ca 20 min). The temperature was next increased to 200 ^{o}C where the viscous liquid had started to swell and was simultaneously auto-ignited. A Large volume of gasses was immediately generated due to the effect of auto-ignition. The evolution of gasses had left behind a voluminous amount of solid powder. The obtained powder was finally calcined at 500 ^{o}C for 4 hr to produce pure zinc oxide (catalyst B).

Results and Discussion

Characterization of zinc oxide nanoparticles

Thermal Gravimetric Analysis

The TGA -DTA profiles displayed by the corresponding metal hydroxides $Zn(OH)_2$ prepared from different methods in temperature range, 25 -1000°C, are illustrated in Fig. 1. The total weight loss of $Zn(OH)_2$ prepared by precipitation method, was (3.007mg) 14.06% ; only small changes are shown either below 200^o C related to evaporation of adsorbed water, or above 350^o C linked with lattice changes (phase transfer). On the other hand, for $Zn(OH)_2$ prepared by auto-ignition method, (1.707 mg) 9.309 % ; the weight loss up to 300^o C represents the removal of adsorbed water and citrate decomposition while (5.872 mg) 32.01 % ; the loss may be referred to the lattice change between 300 and 400^o C, The total weight loss was 41.32% (7.579 mg) as shown in Table 1.

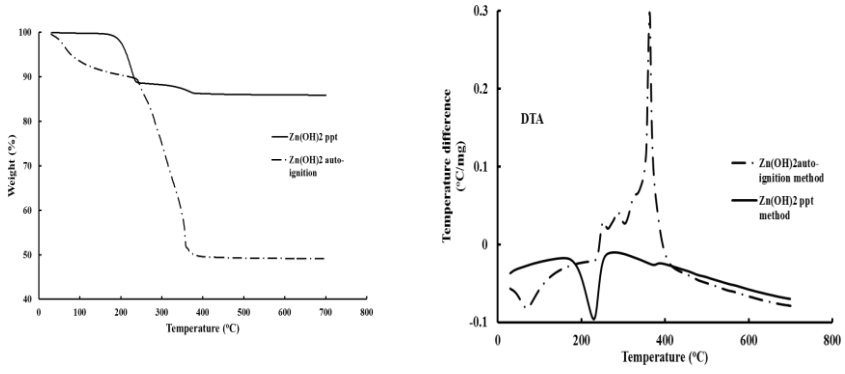

Fig. 1. TGA and DTA curves of prepared $Zn(OH)_2$ by preciptation method and auto-ignition method.

TABLE 1. Thermal analysis and weight losses from thermal analysis of $Zn(OH)_2$ by precipitation and auto-ignition methods.

Components	Components range and % of Wt. loss	
	Water removal ($\leq 200^oC$)	Lattice changes ($300\text{-}400^oC$)
Metal hydroxide of Catalyst A	2.417 (2.491 mg)	11.65 (1.701 mg)
Metal hydroxide of Catalyst B	9.309 (1.707 mg)	32.01 (5.872 mg)

X-Ray Diffraction (XRD)

Figure 2 shows the XRD patterns of the as-synthesized catalysts A and B. From this XRD patterns analysis, we determined peak intensity, position and width, full-width at half-maximum (FWHM) data. All the diffraction patterns indexed to the hexagonal wurtzite structure zincite phase of ZnO[23-26] with crystal lattice 3.902 and 3.900 , respectively, which is in good agreement with the literature values (card No.01-070-2551) and (card No.01-36-1451) respectively.

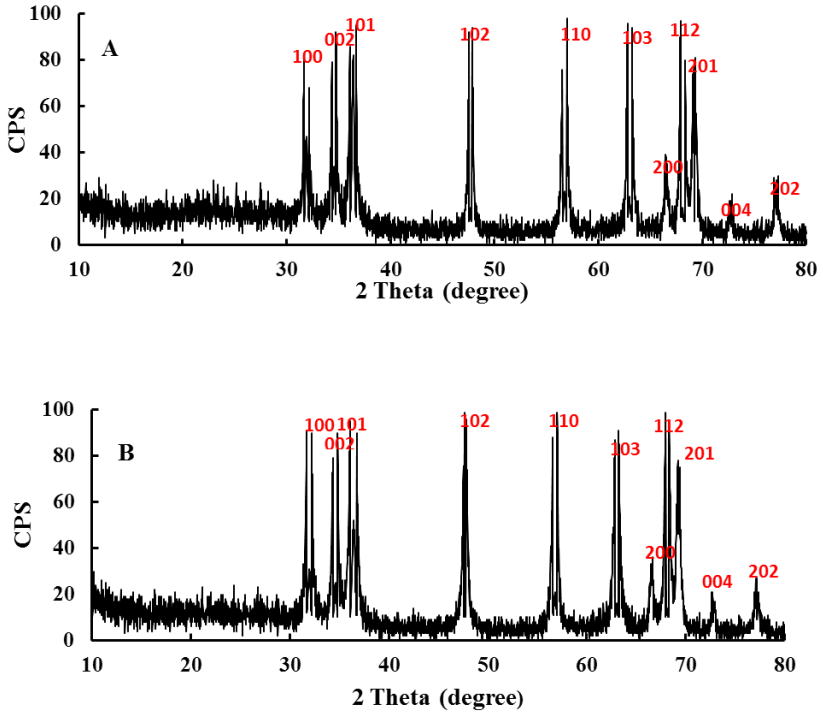

Fig. 2. XRD patterns of ZnO nanoparticles catalyst A and catalyst B.

The diffraction pattern shows the as-prepared nanoparticles was monophasic zincite with rod structures. Both catalysts have exhibited similar spectrums consisting of main reflections centered around 2θ of 31.37°, 34.42°, 36.26°, 47.54°, 56.61°, 62.68°, 66.39°, 67.96°, 69.10°, 72.55°, and 76.97° corresponding to (100), (002), (101), (102), (110), (103), (200), (112), (201), (004), (202). The wurtzite HCP "hexagonal close-pack" structure (Fig. 3), show, each of the two individual atom types forming a sub lattice which is HCP-type. When viewed altogether, the atomic positions are the same as in lonsdaleite (hexagonal diamond). Each atom is tetrahedrally coordinated. The exhibited sharp and intense peaks in the spectrum can explicitly reveal the high crystalline structures of both the prepared catalysts. Also, the absence of any additional peaks confirms the high purity of the prepared nanoparticles. The synthesized ZnO nanoparticle, the crystalline size D_{XRD} was calculated with Scherer's equation[27]: $D = K\lambda/ \beta \cos \theta$, where D is the average size of the crystal; K (the wavelength of X-ray radiation) equal 0.9, λ is the wavelength of X-rays, B is the peak full width at half maximum (FWHM) of the diffraction peak corresponding to plane (101) and θ is the Bragg diffraction angle.

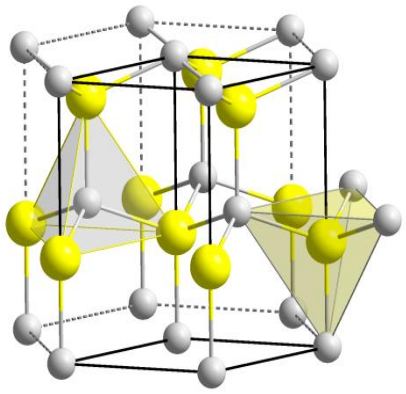

Fig. 3. The wurtzite HCP "hexagonal close-pack" structure.

Surface identifications for ZnO NPs

The surface characteristics of the as-prepared catalysts are illustrated in Table 2. The average particles size of all catalysts, as calculated from the XRD and surface analyzes.

Table 2 shows low surface area values for both catalysts A and B. However, the surface area of catalyst B is higher than that of catalyst A. also, catalyst B had exhibited relatively higher total pore volume, and, a little average pore radius was detected compared with catalyst A. For both catalysts A and B, the detected pores system is uniquely micro-porous structure, since the total pore radius was 1.24 nm and 1.08 nm, respectively. Both catalysts showed similar unit cell according to the following equation: $ao= d_{111}\sqrt{3}$, reported in[28]. Also, they exhibit unlike

average crystal sizes, for example, catalyst A has a bigger particle size than that of catalyst B as calculated from the relationship: $D_{BET}= 6/\rho. S_{BET}$ where ρ is the theoretical density of the powder (5.606 g/cm^3 for ZnO). In line with, catalyst B has presented an average particle size equal to nearly half of the detected grain size of catalyst A, as given by Scherer's equation[28]. This, in turn, could explain the reason behind the slight increase in the surface area value of catalyst B over catalyst A. This also can confirm the good match between the XRD data and the surface characteristics of the synthesized catalysts owing to the linked S_{BET} values to the familiar crystal size by XRD.

TABLE 2. Surface characteristics and particles size values of the as-prepared ZnO NPs.

Catalyst	XRD results		Surface characteristics			
	ao (Å)	D_{XRD} (nm)	S_{BET} (m^2/g)	D_{BET} (nm)	VP (cm^3/g)	r_p (nm)
Catalyst A	3.902	38.62	8.52	30.21	0.012	1.24
Catalyst B	3.900	22.05	12.45	17.19	0.032	1.08

SEM/TEM images

The surface and internal morphology of the as-prepared ZnO structures are investigated respectively through the displayed SEM and TEM; (Fig. 4 & 5) at different magnifications. Both catalysts A and B had exhibited low porous nature (Fig. 4) which is in a high harmony with the acquired total pore volume via the surface analysis. Nevertheless, the two catalysts showed nearly the same surface morphology. Specifically, a non-smooth and non-uniform surface was detected for both catalysts. Moreover, grains of the zinc oxide with some aggregated particles were observed through the given SEM images.

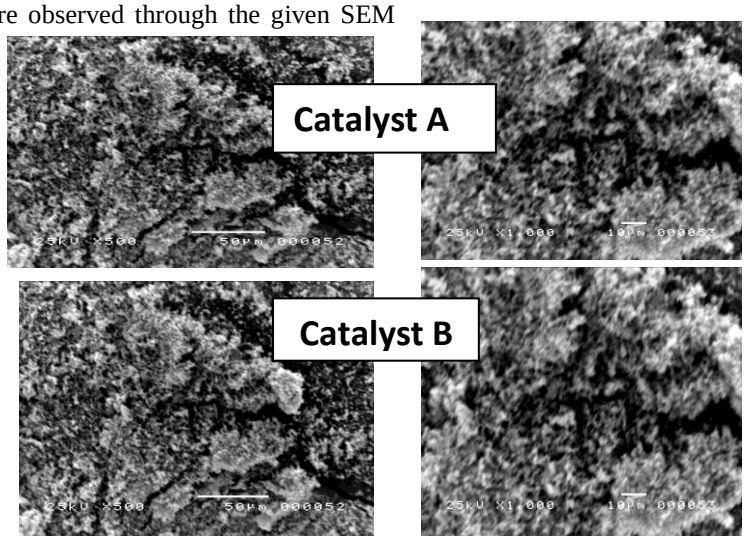

Fig. 4. Surface morphology via SEM micrographs of the as-prepared catalysts A and B.

The displayed TEM micrographs are strongly matching with the data given by the surface area analysis in terms of detecting low porous structure in the crystals of both catalysts. Figure 5 shows nano rod-structures for both catalysts with average sizes of ca 40 and ≥ 22 nm for catalysts A and B, respectively, also shows uniform well-dispersed nanoparticles of the zinc oxides along the whole structure for catalyst B. This can be referred to the usage of the citric acid as a capping agent during the synthesis of catalyst B. The citric acid could help in controlling both the particle size and the crystallization of the obtained ZnO during the preparation. The given measurements by the TEM are genuinely matched with the calculated gain sizes from the XRD data, according to Scherer's equation.

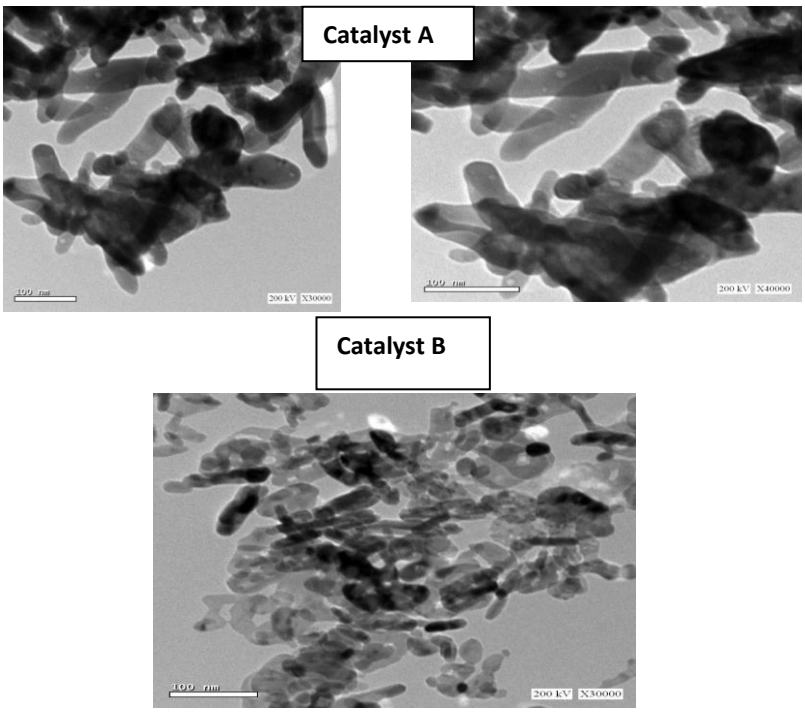

Fig. 5. TEM micrographs of the as-prepared catalysts A and B. UV-Vis absorption spectrum.

UV-Vis absorption spectrum

The influence of the preparation method on the photo-optical of the produced zinc oxides is studied through their capability of absorbing the UV radiation. The spectra of the UV–Visible absorption by the Zn oxides nanoparticles; both catalysts A and B, are shown in Fig. 6. Both catalysts have shown an absorption band at blue shift area (less than 400nm). About the absorption spectra, the effective wavelengths of catalysts A and B are 385 and 355 nm , respectively. In

line with, respective energy band gaps of 3.05 and 3.11 eV for catalyst A and B were detected in Fig.7. The direct band gap of ZnO is estimated from the plot of $(\alpha h\upsilon)^2$ versus $h\upsilon$, where $h\upsilon$ is the photon energy and α is the ratio of the absorption coefficient to the scattering coefficient. These band gaps can explicitly ensure the blue shift which had occurred for the prepared ZnO owing to the inverse proportion of energy gap and wavelength.

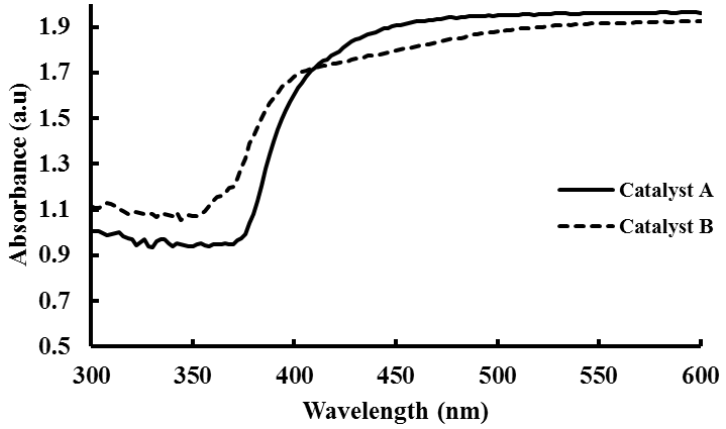

Fig. 6. Electronic absorption of UV-Visible spectra for catalyst A and B.

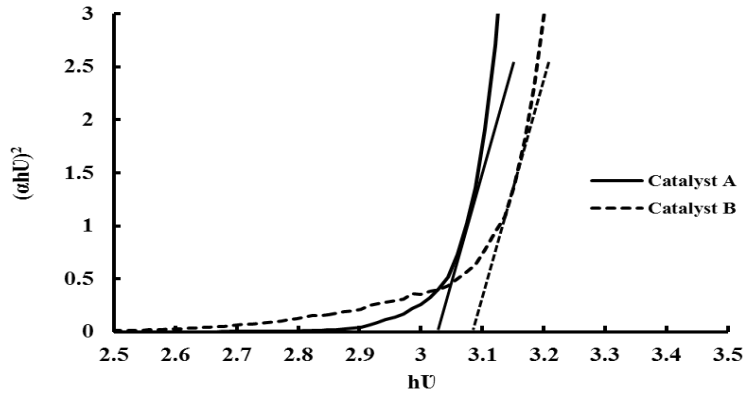

Fig. 7. Plot of $(\alpha hv)^2$ –hv of zinc oxide nanoparticdes.

Photoluminescence Spectrum (PL)

Figure 8 shows the photoluminescence spectrum of as-prepared ZnO NPs by different methods of preparations with excitation wavelength 300 nm at room

temperature. The curve suggests that the electrons in the valence band are transferred to the conduction band, after which the excited electrons are stabilized by photoemission. In general, the PL intensity increases with increasing number of emitted electrons resulting from recombination between excited electrons and holes, leading to a consequent decrease in photo-activity[29,30] . Therefore, there is a strong relationship between the PL intensity and photo-activity. In particular, the band broadening is attributed to the overlapped emission from the higher and lower excited states to the ground states.

So, the PL study was carried out to find the ability of each of catalyst for the photocatalytic reaction. The different wavelengths, for both catalysts are strongly dependent on the energy band gap of each of them. The emission is caused by the radiative recombination of a photo-generated hole with an electron occupying the oxygen vacancy[23.31]. The PL intensity of catalyst B is lower than that of catalyst A which apparently means that recombination of h^+-e^- system in case of catalyst B is slow compared to A. This, in turn, will undoubtedly affect the photocatalytic activity of the synthesized catalysts, specifically, higher activity can be expected for catalyst B which was prepared by auto-ignition method.

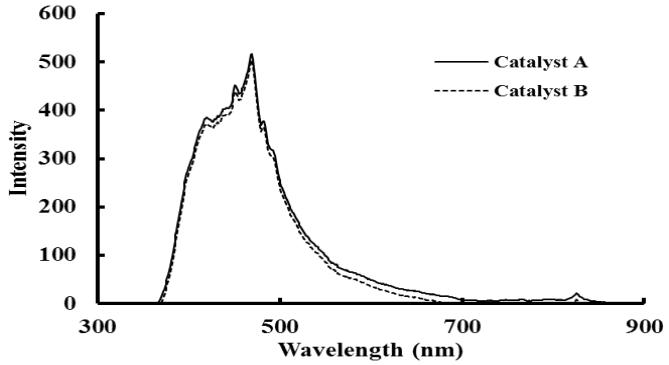

Fig. 8. Room temperature PL spectra of ZnO (NPs) for catalyst A and B.

Conclusions

ZnO nanoparticles have been prepared through precipitation method and auto-ignition method. ZnO NPs were characterized by XRD, SEM, Tem, UV-Vis absorption, and photoluminescence spectroscopy. XRD, surface data and TEM studies confirmed the nanostructures for the as-prepared ZnO nanoparticles. The UV-visible results showed that the absorption wavelength range of the ZnO prepared by two previous methods were extended towards the UV- region (λ is less than 400 nm) with band gap energy 3.05 and 3.11 eV , respectively.

Photoluminescence (PL) spectra proved that ZnO prepared by auto-ignition method was the most active one. This indicated a minimum recombination rate. As a result, they possess the highest photocatalytic activity due to the effective separation of excited electron/holes. These ZnO nanoparticles can be used in different photocatalytic and industrial applications due to its great optical properties.

References

1. **Tokumoto, M. S., Briois ,V., Santilli ,C. V. and Pulcinelli, S. H.,** Preparation of ZnO nanoparticles: Structural study of the molecular precursor.Journal of Sol-Gel Sience and Technology, **26** (1-3), 547-551(2003).

2. **Kumar, P., Panchakarla, L. S., Bhat, S. V., Maitra, U., Subrahmanyam, K. S. and Rao C. N. R.,** Photoluminescence, white light emitting properties and related aspects of ZnO nanoparticles admixed with graphene and gan. *Nanotechnology*, **21**, (38), 385701(2010).

3. **Liu, Y., Pollaor, S. and Wu, Y.,** Electrohydrodynamic processing of p-type transparent conducting oxides, *Journal of Nanomaterials* (2015).

4. **Md Sin, N. D., Fuad Kamel, Alip M. R. I., Mohamad Z. and Rusop, M.,** The electrical characteristics of aluminium doped zinc oxide thin film for humidity sensor applications. *Advances in Materials Science and Engineering* (2011).

5. **Rao, C. N. R. and Govindaraj, A.,** *Nanotubes and Nanowires RSC Nanoscience & Nanotechnology Series*, RSC Publishing: Cambridge, UK, (2005).

6. **Hames, Y., Alpaslan, Z. H., KÃ¶semen,A., San, S. E. and Yerli, Y.,** Electrochemically grown ZnO nanorods for hybrid. *Solar Cell Applications*, **84** (3), 426-431(2010).

7. **Gao, P. X., Ding, Y., Mai, W., Hughes, W. L., Lao, C. and Wang, Z. L.,** Conversion of zinc oxide nanobelts into superlattice-structured nanohelices, *Science*, **309** (5741), 1700-1704(2005).

8. **Topoglidis, E., Cass, A. E. G., O'Regan, B. and Durrant, J. R.,** Immobilisation and bioelectrochemistry of proteins on nanoporous TiO_2 and ZnO films. *Journal of Electroanalytical Chemistry*, **517** (1), 20-27(2001).

9. **Jun, W., Changsheng, X., Zikui, B., Bailin, Z., Kaijin, H. and Run, W.,** Preparation of ZnO -glass varistor from tetrapod zno nanopowders, *Materials Science and Engineering:* B **95**(2), 157-161(2002).

10. **Cheng, X. L., Zhao, H., Huo, L. H., Gao, S. and Zhao, J. G.,** ZnO nanoparticulate thin film: Preparation, characterization and gas-sensing property. *Sensors and Actuators B: Chemical* **102**(2), 248-252(2004).

11. **Sharma, P., Sreenivas, K. and Rao, K. V.,** Analysis of ultraviolet photoconductivity in ZnO films prepared by unbalanced magnetron sputtering, *Journal of Applied Physics*, **93**(7), 3963-3970(2003).

12. **Kamat, P. V., Huehn, R. and Nicolaescu, R.,** Approach for photocatalytic degradation of organic contaminants in water. *The Journal of Physical Chemistry* B **106** (4), 788-794 (2002).

13. **Tokumoto, M. S., Pulcinelli, S. H., Santilli, C. V. and Briois, V. R.,** Catalysis and temperature dependence on the formation of zno nanoparticles and of zinc acetate derivatives prepared by the sol-gel route. *The Journal of Physical Chemistry* B **107** (2), 568-574(2003).

14. **Rataboul, F., Nayral, C. l., Casanove, M.-J., Maisonnat, A. and Chaudret, B.,** Synthesis and characterization of monodisperse zinc and zinc oxide nanoparticles from the organometallic precursor [zn (c 6 h 11) 2]. *Journal of Organometallic Chemistry* **643**, 307-312(2002).

15. **Singhai, M., Chhabra, V., Kang, P. and Shah, D.O.,** Synthesis of ZnO nanoparticles for varistor application using zn-substituted aerosol ot microemulsion. *Materials Research Bulletin*, **32**(2), 239-247(1997).

16. **Okuyama, K. and Lenggoro, I. W.,** Preparation of nanoparticles via spray route. *Chemical Engineering Science*, **58** (3), 537-547(2003).

17. **Moghaddam, A. B., Nazari, T., Badraghi, J. and Kazemzad, M.,** Synthesis of ZnO nanoparticles and electrodeposition of polypyrrole/zno nanocomposite film,. *Int J Electrochem Sci* **4**,(2), 247-257(2009).

18. **Hu, X.-L., Zhu, Y.-J. and Wang, S.-W.,** Sonochemical and microwave-assisted synthesis of linked single-crystalline ZnO rods. *Materials Chemistry and physics* **88** (2), 421-426(2004).

19. **Wei, Y.-L. and Chang, P.-C.,** Characteristics of nano zinc oxide synthesized under ultrasonic condition. *Journal of Physics and Chemistry of Solids*, **69**,(2), 688-692(2008).

20. **Wu, J.-J. and Liu, S.-C.,** Low-temperature growth of well-aligned ZnO nanorods by chemical vapor deposition. *Advanced Materials*,**14** (3), 215(2002).

21. **Zhai, H.-J., Wu, W.-H., Lu, F., Wang, H.-S. and Wang, C.,** Effects of ammonia and cetyltrimethylammonium bromide (ctab) on morphologies of ZnO nano-and micromaterials under solvothermal process. *Materials Chemistry and physics*,**112**(3), 1024-1028(2008).

22. **Bitenc, M., MarinÅ¡ek, M. and Orel, Z. C.,** Preparation and characterization of zinc hydroxide carbonate and porous zinc oxide particles. *Journal of the European Ceramic Society*, **28**(15), 2915-2921(2008).

23. **Zhou J., Zhao F., Wang Y., Zhang Y. and Yang L.,** Size-controlled synthesis of ZnO nanoparticles and their photoluminescence properties. *Journal of Luminescence*, **122**, 195-197(2007).

24. **Wang, Y., Zhang, C., Bi, S. and Luo, G.,** Preparation of ZnO nanoparticles using the direct precipitation method in a membrane dispersion micro-structured reactor. *Powder Technology*, **202**, 130-136**(**1â€“3).

25. **Lucilha, AC., Afonso, R., Silva, P.R.C., Lepre, L.F., Ando, R.M.A.and Dall'Antonia,L.H.,** ZnO prepared by solution combustion synthesis: Characterization and application as photoanode, *Journal of the Brazilian Chemical Society*, **25**, (6), 1091-1100 (2014).

26. **Khoshhesab, Z. M., Sarfaraz, M. and Asadabad, M. A.,** Preparation of ZnO nanostructures by chemical precipitation method. *Synthesis and Reactivity in Inorganic, Metal-Organic, and Nano-Metal Chemistry* ,**41**(7), 814-819(2011).

27. **Herman, R. G., Klier, K., Simmons, G. W., Finn, B. P., Bulko, J. B. and Kobylinski, T. P.,** Catalytic synthesis of methanol from COH_2: I. Phase composition, electronic properties, and activities of the Cu/ ZnO /M_2O_3 catalysts. *Journal of Catalysis*, **56** (3), 407-429(1979).

28. **Sahoo, S. K., Mohapatra, M., Pandey, B., Verma, H. C., Das, R. P. and Anand, S.,** Preparation and characterization of Î±-Fe_2O_3â€“CeO_2composite. *Materials Characterization*, **60**(5), 425-431(2009).

29. **Noh, J. H., Cho, I. S., Lee, S., Cho, C. M., Han, H. S., An, J. S., Kwak, C. H., Kim, J. Y. Jung, H. S. and Lee, J. K.,** Photoluminescence and electrical properties of epitaxial alâ€doped ZnO transparent conducting thin films. *Physica Status Solidi (a)* **206**(9), 2133-2138(2009).

30. **Yun, E.-J., Jung, J. W., Cheon, C. I., Kim, J. S., Han, Y. H., Kim, M.-W. and Lee, B. C.,** P-type conduction in room-temperature high-energy electron-irradiated ZnO thin films. *Journal of Materials Research*, **24**(05), 1785-1790(2009).

31. **Huang, M.H., Wu, Y., Feick, H., Tran, N., Weber, E. and Yang, P.,** Catalytic growth of zinc oxide nanowires by vapor transport. *Advanced Materials* **13**(2), 113-116(2001).

(*Received* 13/4/2016;
accepted 20/4/2016)

تحضير وتوصيف أكسيد الزنك النانوني ذات مسام صغيره لتطبيقها فى التحفيز الضوئى

أسماء سعيد مرشدى[1]، أحمد متولى النجار[1]، سحر محمود توفيق[1]، عمر إبراهيم سيف الدين [1]، سناء إبراهيم حسن[1] و أحمد إسماعيل هاشم[2]
[1]معهد بحوث البترول و [2]قسم الكيمياء – كلية العلوم – جامعة عين شمس -القاهرة– مصر .

تم تحضير أكسيد الزنك النانونى عن طريق عمليه الترسيب الكيميائى و طريقه الإشتعال الذاتى من نترات الزنك هيدرات. تم وصف الماده بإستخدام التحليل الحرارى ، حيود الأشعة السينية ، المجهر الإلكتروني ، وإنبعاثات الإلكترون المجهري ، والأشعة فوق البنفسجية – البصرية ، و التحليل الطيفي الضوئى. أظهرت الأشعه السينيه لكلا من المواد الحفازه التى تم تحضريها بالطريقتين عن تكوين أكسيد الزنك النانونى التركيب ذات هيكل سداسى. أوضحت نتائج المجهر الإليكترونى الشكل الخارجى للأوكسيد المتكون وأيضا حجم الجسيمات داخل أكسيد الزنك النانونى التركيب. الأشعه فوق بنفسجيه أظهرت ان أوكسيد الزنك الذى تم تحضيره بطريقه الترسيب الكيميائى له إمتصاص فى منطقه الأشعه البنفسجيه عند طول موجى 385 نانومتر بينما الذى تم تحضيره بطريقه الإشعال الذاتى له إمتصاص عند طول موجى 355 نانومتر. التحليل الطيفى الضوئى أثبت ان أكسيد الزنك الذى تم تحضيره بطريقه الإشعال الذاتى هو الأكثر نشاطا حيث أنه يمتلك معدل أقل فى إتحاد (الإليكترون –الثقوب) لذلك فانها تمتلك أعلى نشاط ضوئى بسبب الفصل الفعال بين (الإليكترون –الثقوب). لذلك فإن أكسيد الزنك الذى تم تحضيره بطريقه الإشعال الذاتى يمكن إستخدامه فى التطبيقات الضوئيه والصناعيه بسبب الخصائص البصريه الهائله .